Terephthalic Acid Intercalation Strengthens NiFe-Layered Double Hydroxide for Durable and Efficient Seawater Electrolysis

Xinghong Li,[a] Yuxin Zhu,[a] Yi Huang,[a] Yaohai Cai,[a] Kai Liu,[a] Lei Wang,[a] Zhenbo Wang,[b] Deliang Zhu [c,*] and Dong Liu [a,*]

[a] Guangdong Provincial Key Laboratory of New Energy Materials Service Safety, College of Materials Science and Engineering, Shenzhen University, Shenzhen 518060, China

[b] State Key Laboratory of Space Power-Sources, MIIT Key Laboratory of Critical Materials Technology for New Energy Conversion and Storage, MOE Engineering Research Center for Electrochemical Energy Storage and Carbon Neutrality in Cold Regions, School of Chemistry and Chemical Engineering, Harbin Institute of Technology, Harbin 150001, China.

[c] Guangdong Research Center for Interfacial Engineering of Functional Materials, Guangdong Provincial Key Laboratory of New Energy Materials Service Safety, College of Materials Science and Engineering, Shenzhen University, Shenzhen, Guangdong 518060, China.

Corresponding authors
Dong Liu, email: dongliu@szu.edu.cn
Deliang Zhu, email: dlzhu@szu.edu.cn

1 Experimental Section

1.1. Materials

The following materials were employed in this study. Nickel foam (NF); hydrochloric acid (36 wt.%, Sinopharm Chemical Reagent Co., Ltd); acetone (≥99.5%, Sinopharm Chemical Reagent Co., Ltd), ethanol, and deionized water with a resistivity of 18.2 MΩ were utilized in all experiments. Key chemicals, including nickel nitrate ($Ni(NO_3)_2 \cdot 6H_2O$, ≥99.0%), iron(III) nitrate ($Fe(NO_3)_3 \cdot 9H_2O$, ≥99.0%), and terephthalic acid (TPA, ≥99.0%) were purchased from Shanghai Aladdin Biochemical Technology Co., Ltd. N,N-Dimethylformamide (DMF, ≥99.0%), potassium hydroxide (KOH, ≥85.0%), and commercial RuO_2 were obtained from Shandong Ke Yuan Biochemical Co., Ltd. Additionally, seawater was sourced from the South China Sea (Shenzhen Bay).

1.2. Synthesis of NiFe-LDH(TPA)

As a representative synthesis, the electrodeposition was conducted in a standard three-electrode configuration using a Pt counter electrode and an Ag/AgCl reference electrode (saturated KCl). A nickel foam (NF) substrate (1 × 2 cm^2) served as the working electrode. Prior to deposition, the NF was sequentially ultrasonicated in acetone, dilute HCl, and ethanol for 10 minutes each, followed by rinsing with

deionized water and ethanol, and subsequent drying at 80°C for 30 minutes. The precursor solution was prepared as follows. First, 3 mmol of $Fe(NO_3)_3 \cdot 9H_2O$ and 4.5 mmol of $Ni(NO_3)_2 \cdot 6H_2O$ were dissolved in 20 mL of deionized water under magnetic stirring for 30 min to obtain a homogeneous metal salt solution. Separately, 0.8 mmol of TPA was dissolved in 10 mL of DMF by stirring for 30 min, yielding a clear organic solution. The two solutions were then mixed and stirred vigorously for 1 h to form a stable and uniform electrodeposition bath. Electrodeposition was performed at a constant potential of -1.2 V for 1600 seconds, yielding TPA-modified ultrathin NiFe-layered double hydroxide nanosheets (designated as NiFe-LDH(TPA)). The resulting electrode was thoroughly rinsed with ethanol and deionized water, then dried at 80°C for 40 minutes. The effective deposition area was maintained at 1 × 1.5 cm^2 throughout the process.

1.3. Synthesis of NiFe-LDH

The synthesis of NiFe-layered double hydroxide (NiFe-LDH) followed a procedure analogous to that of NiFe-LDH(TPA), with the key modification being the exclusion of TPA from the deposition solution. The electrochemical deposition solution was prepared by dissolving 3 mmol $Fe(NO_3)_3 \cdot 9H_2O$ and 4.5 mmol $Ni(NO_3)_2 \cdot 6H_2O$ in a mixed solvent consisting of 20 mL deionized water and 10 mL DMF, followed by stirring for 1 h. All other experimental parameters, including the electrodeposition potential (-1.2 V), duration (1600 s), and post-treatment conditions, were maintained identical to those employed for the preparation of NiFe-LDH(TPA) to ensure comparative validity.

1.4. Synthesis of RuO_2

For the preparation of the RuO_2 reference electrode, a slurry was prepared by dispersing 20 mg of RuO_2 powder and 60 μL of Nafion solution in a mixed solvent containing 540 μL of absolute ethanol and 400 μL of deionized water, followed by sonication for 30 min. The resulting homogeneous ink was then drop-cast onto a nickel foam substrate and dried in air overnight.

1.5. Physical characterizations

Scanning electron microscopy (SEM) analyses were conducted using a Hitachi S-8200. Transmission electron microscopy (TEM) and high-resolution transmission electron microscopy (HR-TEM) images were captured with a JEM2100UHR instrument. X-ray diffraction (XRD) measurements were performed on an X'Pert PRO MPD system. FT-IR spectra were acquired on a Thermo Nicolet Nexus 670 spectrometer. X-ray photoelectron spectroscopy (XPS) assessments were carried out using an AXIS SUPRA equipped with a monochromatic Al Kα source at 15 mA and 14 Kv and the C ls peak (284.8 eV) of contaminated carbon was used to calibrate the binding energy. In-situ Raman spectra were collected with an Invia Qontor Raman spectroscopy system utilizing a 532 nm laser. UV-vis diffuse reflectance spectra (DRS) were recorded using the SHIMADZU UV-3600iPlus spectrophotometer.

1.6. Electrochemical measurements

Electrochemical evaluations of all samples were performed using CHI660E and DH7006B-2 stations in an alkaline seawater electrolyte, prepared by adding 1 M KOH to natural, unpurified seawater collected from the South China Sea. A Hg/HgO electrode and a graphite rod served as the reference and counter electrodes, respectively, for the oxygen evolution reaction (OER).

All the prepared samples were utilized as working electrodes. Potentials in these experiments were adjusted to the reversible hydrogen electrode (RHE) standard using the formula: E_{RHE}= E + 0.098 V + 0.0591 × pH. The electrocatalytic performance was assessed in various electrolytes: 1.0 M KOH and a 1.0 M KOH seawater solution. Linear sweep voltammetry (LSV) with a scan rate of 5 mV s^{-1} was employed to evaluate the OER activities. Tafel slopes were determined from the linear regions of the Tafel plots using the Tafel equation upon LSV curves without iR compensation. Cyclic voltammetry (CV) tests were performed at varying scan rates (20, 40, 60, 80, and 100 mV s^{-1}) to determine the double-layer capacitance (C_{dl}) of the catalysts. Electrochemical impedance spectroscopy (EIS) was conducted across a frequency range of 0.01 kHz to 1000 kHz. Long-term stability was assessed via chronopotentiometry at room temperature.

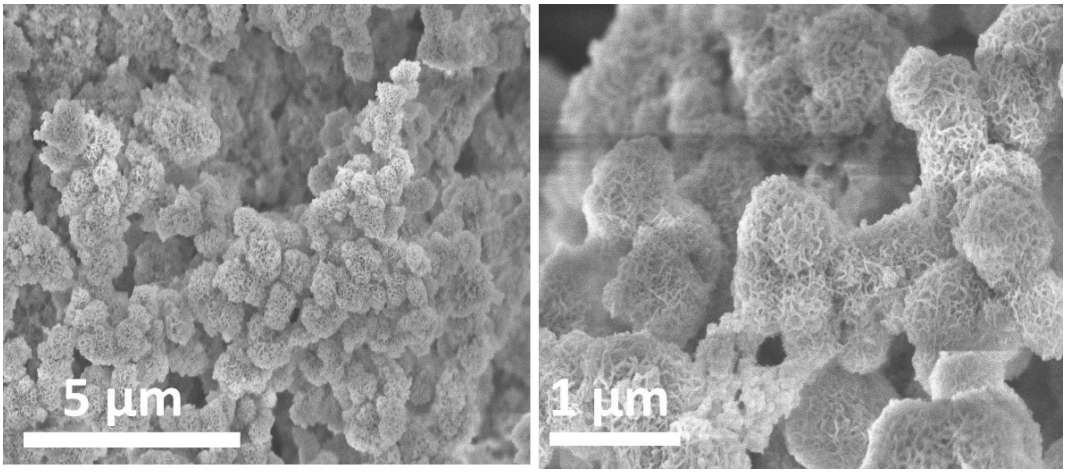

Figure S1. SEM images of NiFe-LDH(TPA).

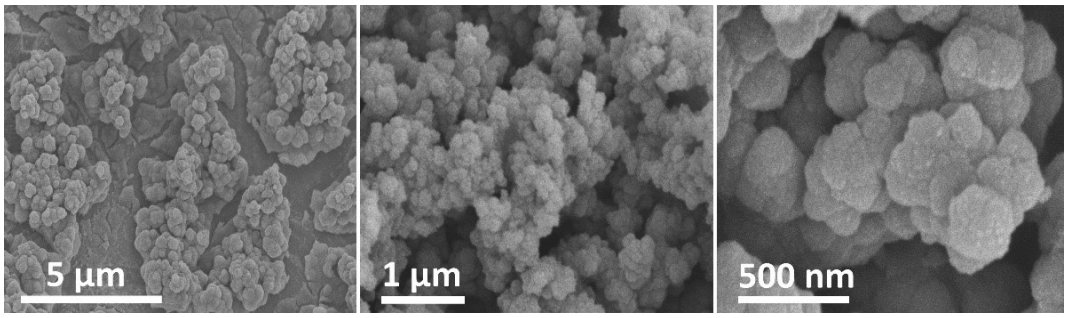

Figure S2. SEM images of NiFe-LDH.

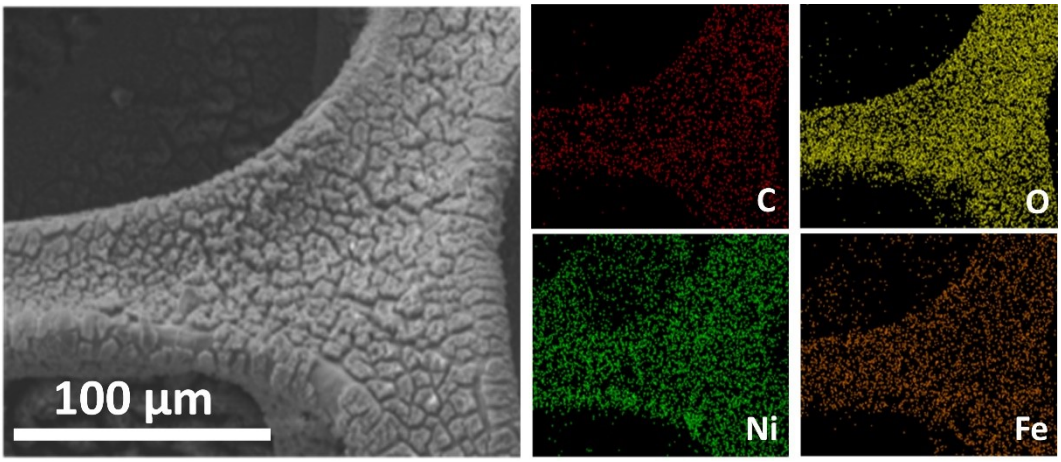

Figure S3. SEM image of NiFe-LDH(TPA) with EDS images

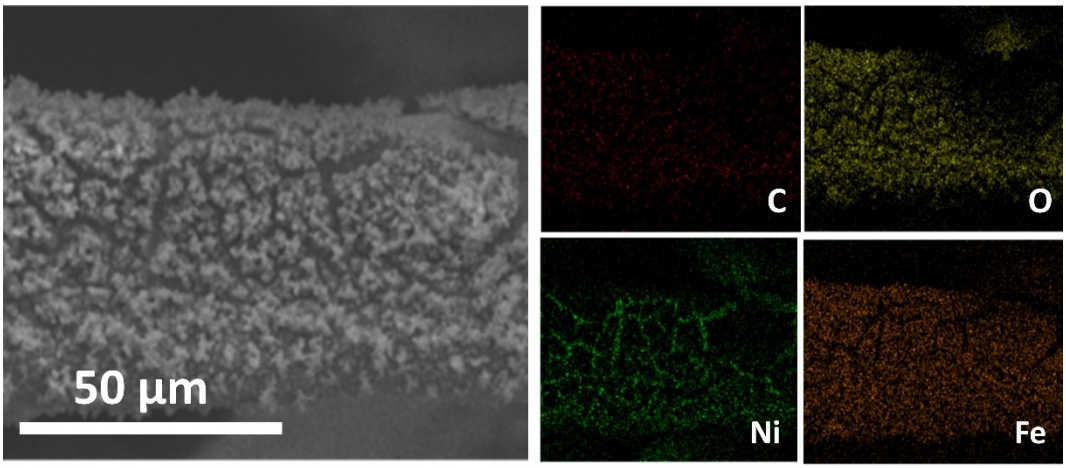

Figure S4. SEM image of NiFe-LDH with EDS images

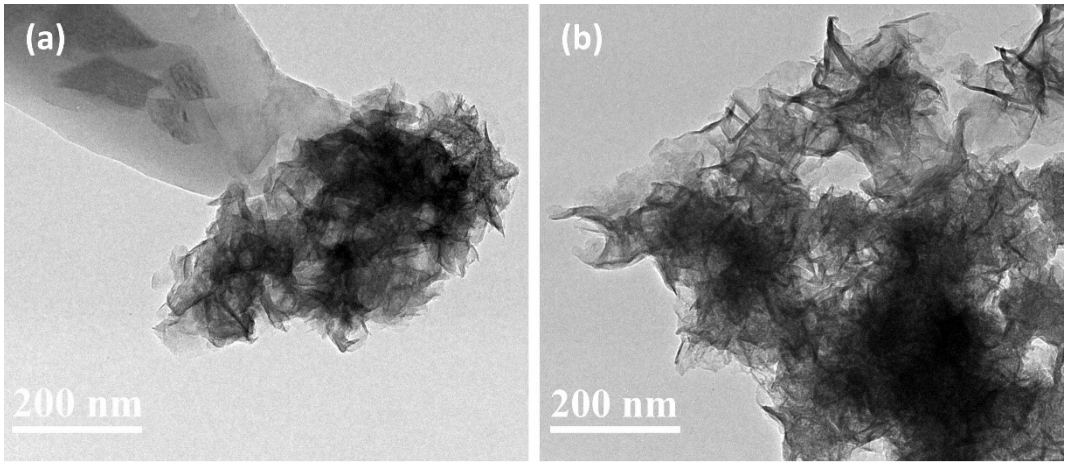

Figure S5. TEM images of (a) NiFe-LDH and (b) NiFe-LDH(TPA)

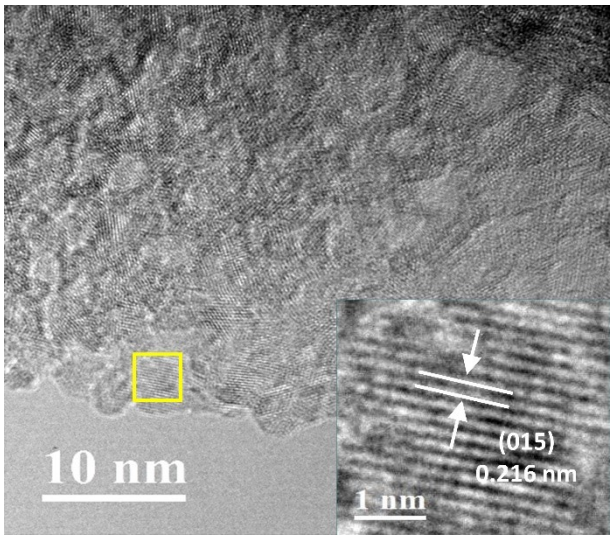

Figure S6. HRTEM images of NiFe-LDH

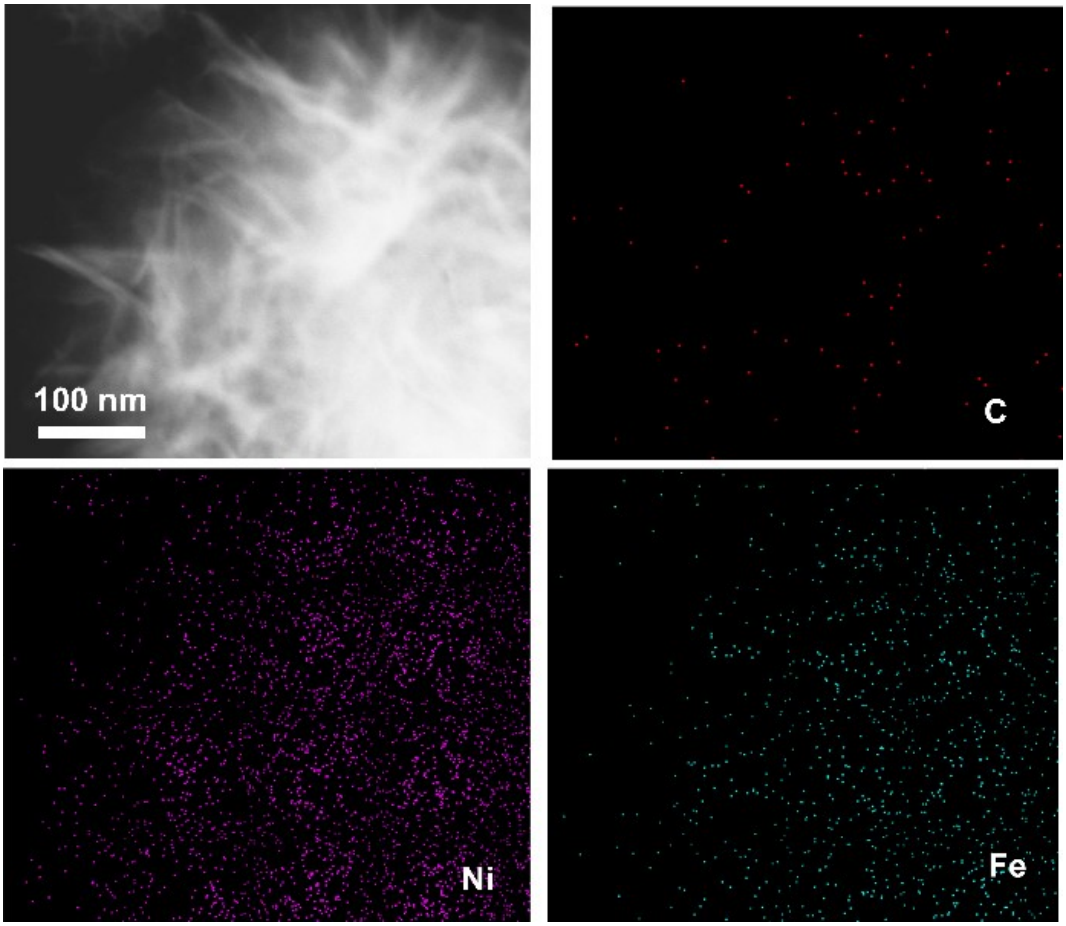

Figure S7. Corresponding EDX elemental mapping of NiFe-LDH(TPA).

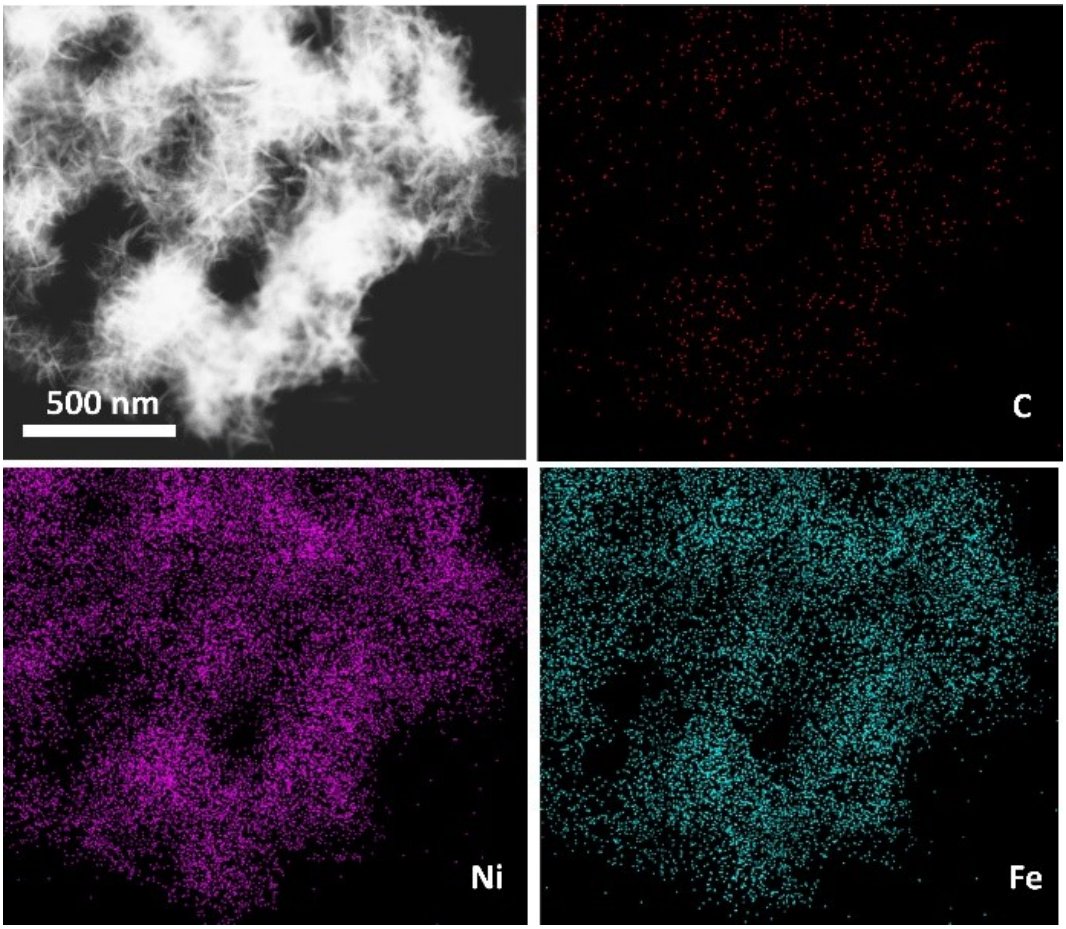

Figure S8. Corresponding EDX elemental mapping of NiFe-LDH.

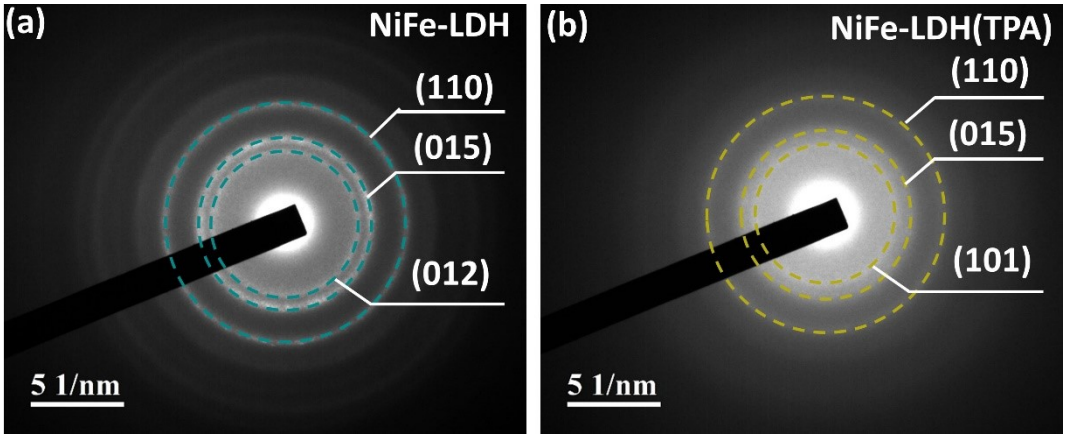

Figure S9. Selected-area electron diffraction (SAED) patterns of (a) NiFe-LDH and (b) NiFe-LDH(TPA).

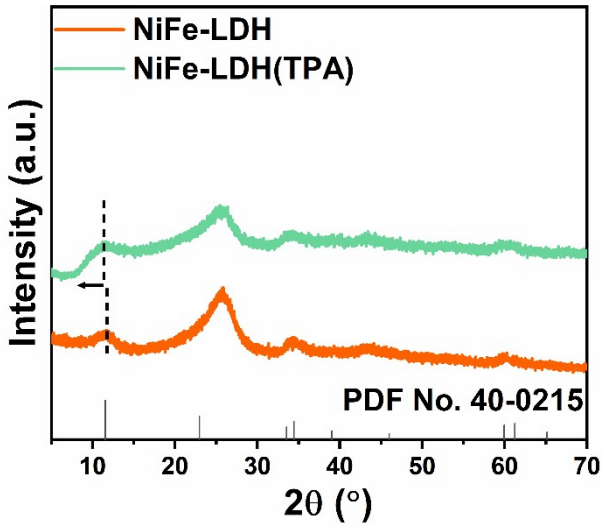

Figure S10. XRD patterns of NiFe-LDH and NiFe-LDH(TPA).

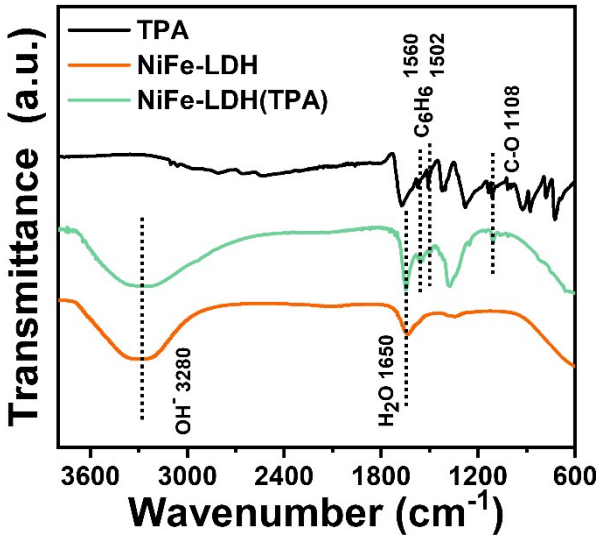

Figure S11. FT-IR spectra of TPA, NiFe-LDH, and NiFe-LDH(TPA).

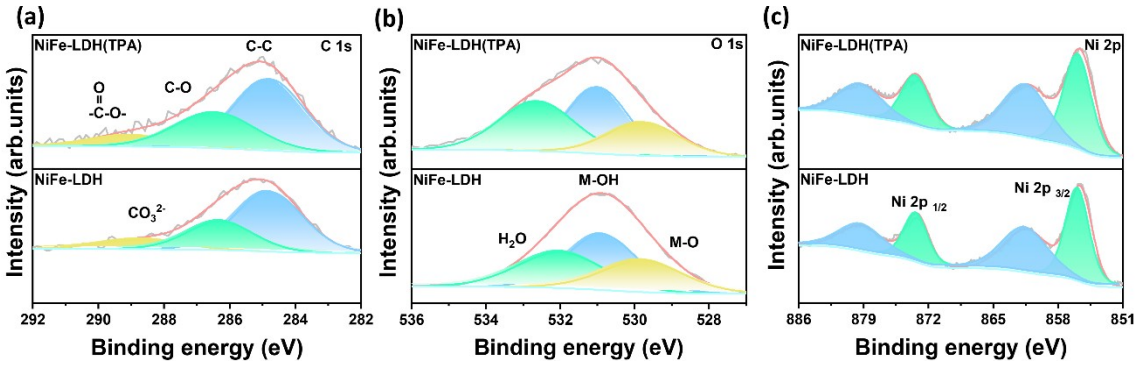

Figure S12. High-resolution XPS spectra of (a) C1 s, (b) O1 s, and c) Ni 2p for NiFe-LDH and NiFe-LDH(TPA).

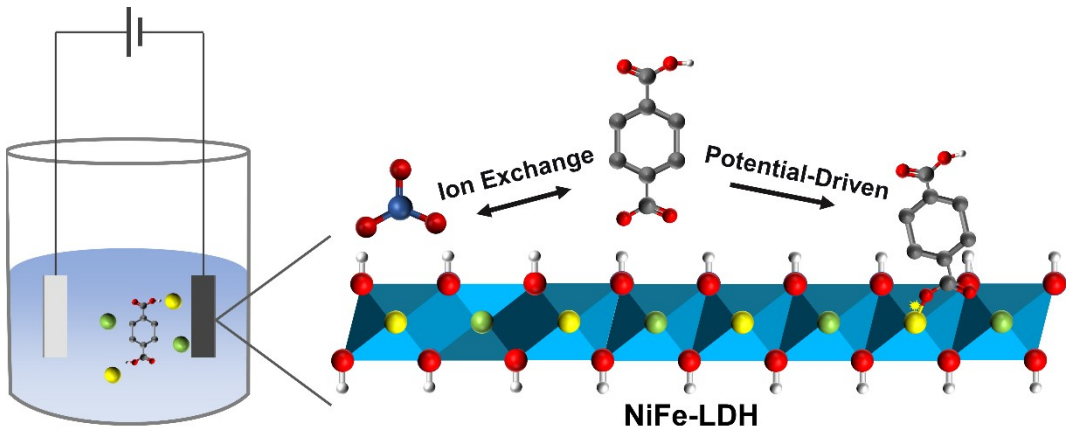

Figure S13. Schematic illustration of the one-pot synthesis and C-O-Fe bonding in TPA-intercalated NiFe-LDH.

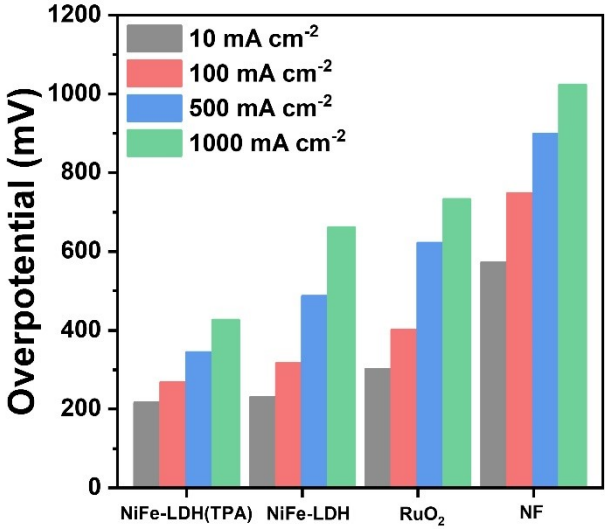

Figure S14. Comparison of the overpotentials required to reach specific current densities for NiFe-LDH(TPA), NiFe-LDH, RuO_2, and NF during OER measurements in 1 M KOH seawater electrolyte.

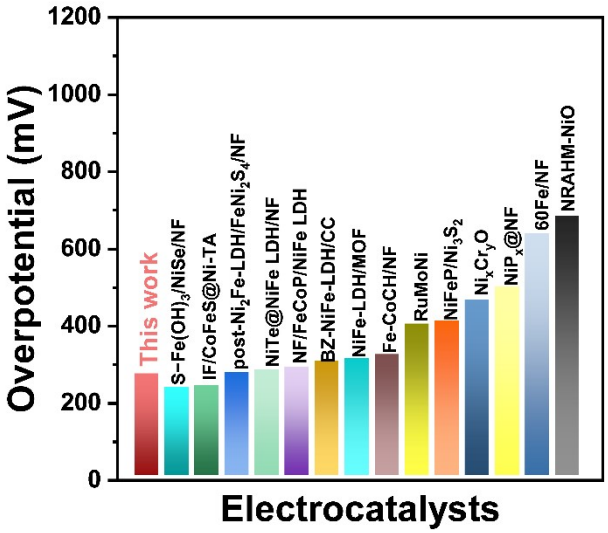

Figure S15 Comparison of current densities at 10 mV for the different catalysts.

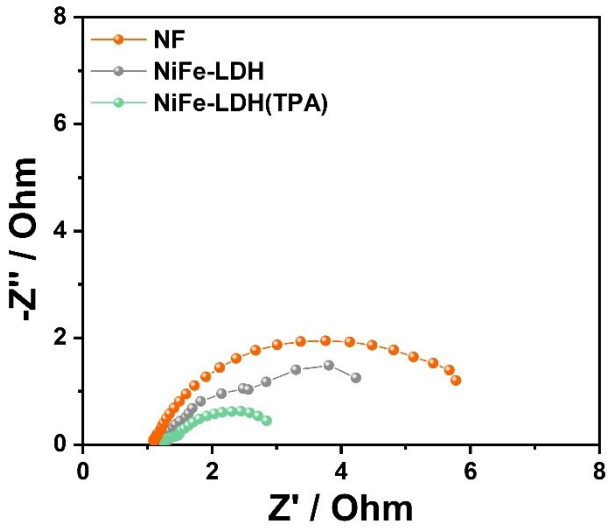

Figure S16. Nyquist plots of NiFe-LDH(TPA), NiFe-LDH and NF.

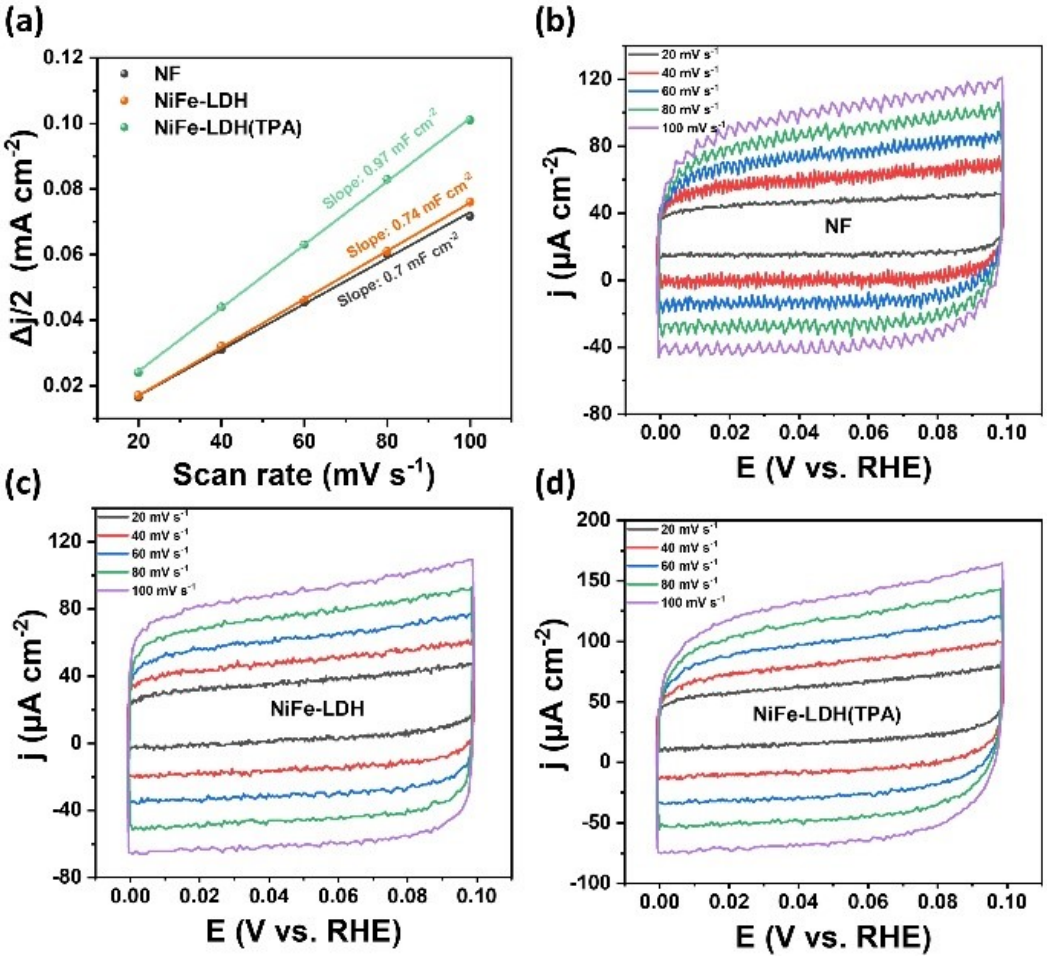

Figure S17. (a) The double-layer capacitance of NiFe-LDH(TPA), NiFe-LDH and NF (b-d) cyclic voltammograms of NiFe-LDH(TPA), NiFe-LDH and NF at scan rates in the range of 20-100 mV s^{-1}, respectively.

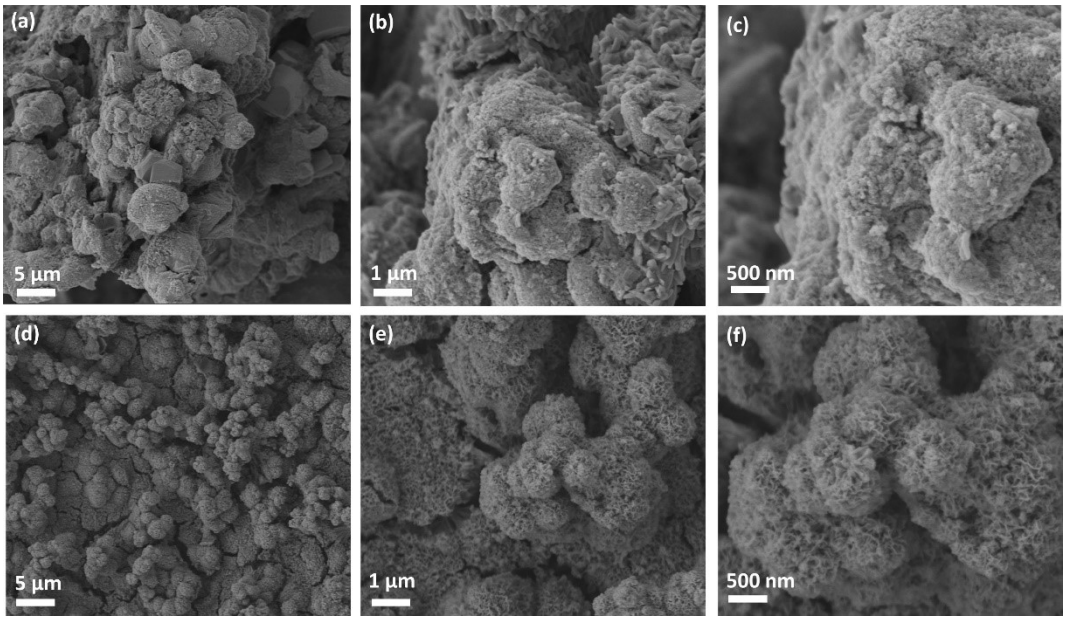

Figure S18. SEM image of (a-c)NiFe-LDH and (d-f)NiFe-LDH(TPA) after durability test in alkaline seawater.

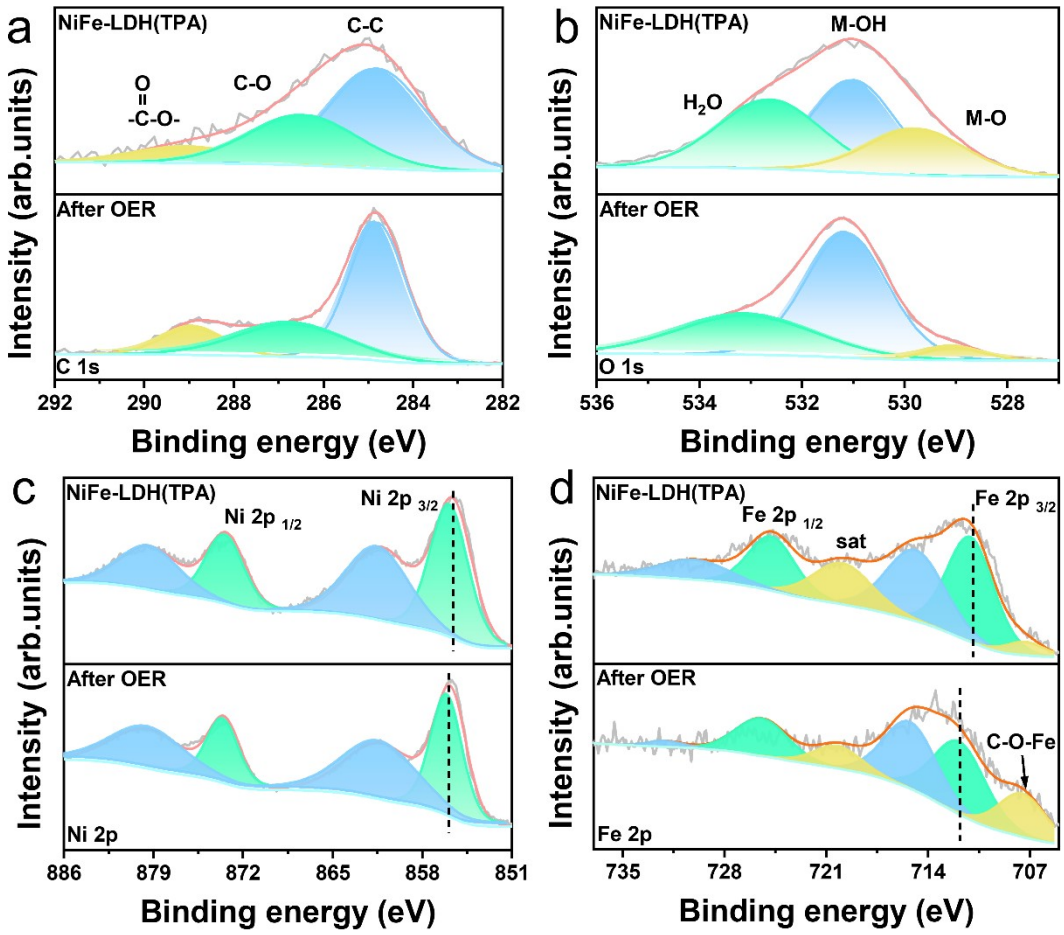

Figure S19. High-resolution XPS spectra of (a) C 1s, (b) O 1s, (c) Ni 2p, and (d) Fe 2p for NiFe-LDH(TPA) before and after OER.

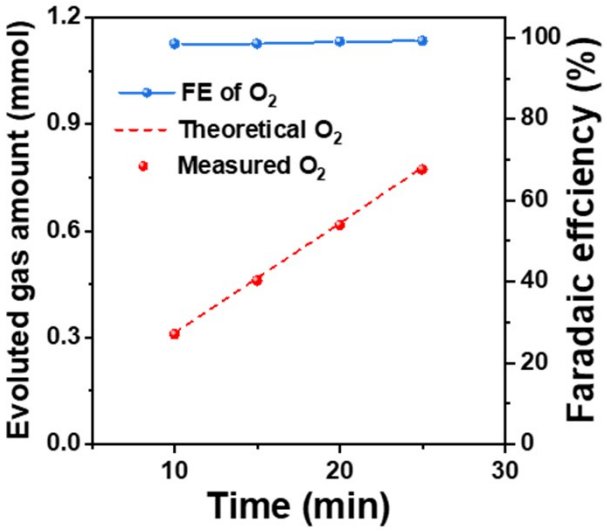

Figure S20. Theoretical and experimental O_2 evolution, and calculated Faradaic efficiency (FE) of NiFe-LDH(TPA).

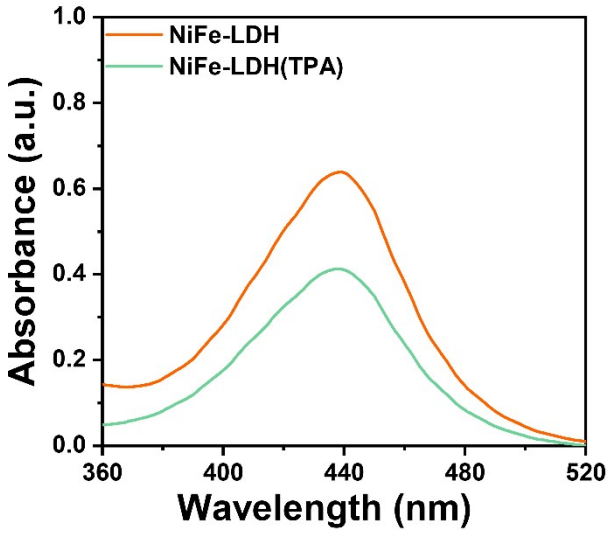

Figure S21. UV–vis absorption spectra of NiFe-LDH and NiFe-LDH(TPA).

Table S1. Comparison of OER catalytic performance for seawater oxidation between NiFe-LDH(TPA) and recently reported self-supported catalysts.

Electrocatalysts	Electrolyte	η_{100}*	Reference
NiFe-LDH(TPA)	1M KOH + seawater	267	This work
IF/CoFeS@Ni-TA	1M KOH + seawater	237	*Applied Catalysis B: Environment and Energy*, 2025, **379**, 125669
S−Fe(OH)$_3$/NiSe/NF	1M KOH + seawater	232	*ACS Appl. Nano Mater.*, 2024, **7**, 3960–3967
NiFeP/Ni_3S_2	1M KOH + seawater	406	*Applied Catalysis B: Environment and Energy*, 2024, **352**, 124028
60Fe/NF	1M KOH + seawater	635	*Advanced Energy Materials*, 2023, **13**, 2301921
NiP_x@NF	1M KOH + seawater	494	*Small*, 2023, **19**, 2205689
NRAHM-NiO	1M KOH + seawater	680	*ACS Catal.*, 2023, **13**, 5516–5528
RuMoNi	1M KOH + seawater	397	*Nat Commun*, 2023, **14**, 3607
Ni_xCr_yO	1M KOH + seawater	460	*Angewandte Chemie International Edition*, 2023, **62**, e202309854
BZ-NiFe-LDH/CC	1M KOH + seawater	300	*Nano Research Energy*, 2022, **1**, 9120028
NiTe@NiFe LDH/NF	1M KOH + seawater	277	*iScience*, 2024, **27**, 108736
Fe-CoCH/NF	1M KOH + seawater	317	*Inorg. Chem.*, 2023, **62**, 11746–11750
NiFe-LDH/MOF	1M KOH + seawater	307	*Nano Res.*, 2023, **16**, 8945–8952
NF/FeCoP/NiFe LDH	1M KOH + seawater	285	*International Journal of Hydrogen Energy*, 2025, **118**, 102–112
post-Ni_2Fe-LDH/$FeNi_2S_4$/NF	1M KOH + seawater	271	*Inorg. Chem.*, 2023, **62**, 11746–11750

*η100 represent the overpotentials required to attain j of 100 mA cm^{-2}.